

Cumulants from fluctuating width of rapidity distribution

Michał Barej^{*} and Adam Bzdak[†]

AGH University of Science and Technology, Faculty of Physics and Applied Computer Science, 30-059 Kraków, Poland



(Received 3 April 2023; accepted 15 June 2023; published 12 July 2023)

In relativistic heavy-ion collisions, the longitudinal fluctuations of the fireball density caused, e.g., by fluctuations in the number of stopped baryons result in event-by-event modifications of the shape of the proton rapidity density distribution. The multiparticle rapidity correlation functions due to the varying distribution width of the proton rapidity density in central Au + Au collisions at low energies are derived. The cumulant ratios are calculated and discussed in the context of the recent STAR Collaboration results. We find that for small fluctuations in the width of the proton rapidity distribution, the cumulant ratios are independent of the underlying width distribution. It is also emphasized that the cumulant ratios strongly depend on the size of the rapidity interval.

DOI: [10.1103/PhysRevC.108.014907](https://doi.org/10.1103/PhysRevC.108.014907)

I. INTRODUCTION

In relativistic heavy-ion collisions, a very hot (about 10^{12} K) medium, the fireball is created in a tiny volume. Its initial shape asymmetry is reflected in the measured spectra of produced particles. The azimuthal asymmetry is broadly studied using the Fourier decomposition. In this context, the Fourier coefficients are interpreted as harmonic flows, including elliptic flow, triangular flow, and others [1,2]. However, also the long-range longitudinal correlations can be understood as a reflection of the fireball rapidity density fluctuations [3]. These fluctuations result in a nontrivial rapidity correlation function [4]. This function contributes to the proton or baryon number factorial cumulants and cumulants which are potentially very promising in the search for the predicted phase transition and critical point between hadronic matter and quark-gluon plasma [5–26]. Therefore, it is interesting to better understand the correlations related to longitudinal fluctuations.

The longitudinal fluctuations might be affected by the baryon-stopping effect. Indeed, at high energies, baryons are produced as baryon-antibaryon pairs, satisfying the baryon number conservation. At lower energies (at which the phase transition might happen), fewer pairs are created and the greater baryon density is obtained when more incoming baryons are stopped in the specific bin of rapidity. Clearly, a change in the number of stopped baryons in the midrapidity region modifies the fireball density, as well as it should be reflected in the baryon multiplicity cumulants. Therefore, the dynamics of baryon stopping is another source of fluctuations that has to be taken into account.

The measured proton rapidity density distribution is averaged over many events. In particular, there may be

event-by-event fluctuations of the width of the distribution (described by the standard deviation) even if the total number of particles remains the same. The varying numbers of baryons stopped at different rapidity bins may be qualitatively consistent with the picture of width fluctuations.

So far, the longitudinal fluctuations have been studied using the formalism in which the single-particle rapidity density distribution is expanded into orthogonal polynomials [4,27–29]. The coefficients of this expansion have been measured by the ATLAS Collaboration at different collision energies and different colliding systems [30]. This topic has been also addressed by the ALICE Collaboration [31,32]. The width fluctuations of the single-particle rapidity density distribution modify the second-order coefficient in the orthogonal polynomials formalism [4].

In this paper, a new approach that focuses on width fluctuations is proposed. The analytic method to extract the multiparticle rapidity correlation functions from these fluctuations is derived. The correlation functions are used to calculate the corresponding factorial cumulants and cumulants. Different possible characteristics of the width fluctuations are explored. In central Au + Au collisions at low energies, the proton rapidity density distribution is well described by the Gaussian function as seen, e.g., from the recent STAR data [33]. Close to $y = 0$, it can be approximated by the quadratic function. For higher energies, already slightly below 10 GeV, the bimodal structure of the distribution becomes visible and a single Gaussian function is only a rough approximation. However, the goal of this paper is to draw attention and estimate the effect of width fluctuations rather than give precise results.

This paper is organized as follows: In the next section, the general method of deriving multiparticle rapidity correlation functions from the width fluctuations is presented. Then, this method is applied to the quadratic single-particle rapidity density distribution with different width probability distributions. In the subsequent section, the examples of cumulant ratios are calculated and discussed in the context of the corresponding

^{*}michal.barej@fis.agh.edu.pl

[†]adam.bzdak@fis.agh.edu.pl

STAR measurements. We also show that the results are significantly affected by the size of the rapidity interval (e.g., $-0.5 < y < 0$ vs $|y| < 0.5$). Finally, the comments and summary are presented. Higher-order cumulants are discussed in the Appendix.

II. FACTORIAL CUMULANTS FROM WIDTH FLUCTUATIONS

Let $\varrho(y)$ be a single-particle rapidity density distribution. Suppose the width of this distribution described by the standard deviation σ fluctuates from event to event. The measured distribution $\varrho_{\text{meas}}(y)$ is $\varrho(y)$ averaged over σ . Similarly, $\varrho_{\text{meas},2}(y_1, y_2)$ is a two-particle rapidity density distribution averaged over σ . Then, we construct a two-particle rapidity correlation function originating from the width fluctuation. Following the same reasoning, we calculate higher-order multiparticle rapidity correlation functions.

Suppose $\varrho(y)$ is given by the normal distribution,

$$\varrho(y) = \frac{N_t}{\sqrt{2\pi}\sigma} \exp\left(-\frac{y^2}{2\sigma^2}\right), \quad (1)$$

where $N_t = \int_{-\infty}^{+\infty} dy \varrho(y)$ is the total number of particles. This function is valid for proton rapidity density distribution in central low-energy collisions [33]. For $y \approx 0$ (the midrapidity region), this distribution can be approximated by the quadratic function

$$\varrho(y) \approx \frac{N_t}{\sqrt{2\pi}\sigma} \left(1 - \frac{y^2}{2\sigma^2}\right). \quad (2)$$

We assume that σ (representing the width of the single-particle rapidity density distribution) fluctuates from event to event, being a random variable following the probability distribution, $p(\sigma)$, where $\int_0^{+\infty} d\sigma p(\sigma) = 1$. The average value of σ will be denoted by σ_0 :

$$\sigma_0 \equiv \langle \sigma \rangle = \int_0^{+\infty} d\sigma \sigma p(\sigma). \quad (3)$$

To emphasize the variability of the σ parameter, we denote the rapidity distribution (1) and (2) as $\varrho(y, \sigma)$. In Fig. 1, we show an example of how a change of σ modifies the rapidity distribution, using the values of the parameters that are later used in our examples. Clearly, an increase of σ makes the distribution wider, whereas a decrease of σ , makes the distribution narrower. As seen from the figure, the chosen interval $y \in [-0.5, 0.5]$ is so narrow that $\varrho(y, \sigma)$ with different σ look like a single distribution that is rescaled by different factors.

The measured (averaged over σ) single-particle rapidity density distribution $\varrho_{\text{meas}}(y)$ is obtained as

$$\varrho_{\text{meas}}(y) = \int_0^{+\infty} d\sigma \varrho(y, \sigma) p(\sigma). \quad (4)$$

In the limiting case of $p(\sigma) = \delta(\sigma - \sigma_0)$, where δ is the Dirac δ function, $\varrho_{\text{meas}}(y)$ becomes $\varrho(y; \sigma = \sigma_0)$. We note that the total number of particles, say baryons, $N_t = \int_{-\infty}^{+\infty} dy \varrho_{\text{meas}}(y)$ is unchanged.

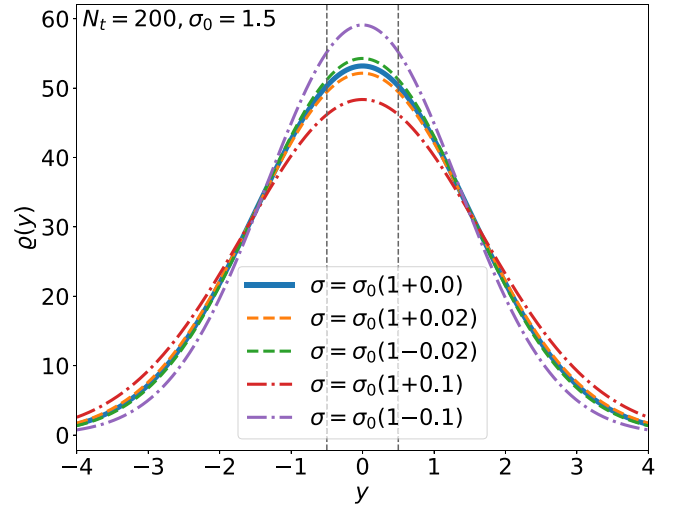


FIG. 1. Proton rapidity density distribution (1) with different values of σ . N_t and σ_0 values are roughly estimated to correspond to proton distribution from central Au + Au collisions at 7.7 GeV, see Sec. III. The vertical dashed lines show the calculation (measurement) range $y \in [-0.5, 0.5]$.

Similarly, the averaged two-particle rapidity density distribution reads

$$\varrho_{\text{meas},2}(y_1, y_2) = \int_0^{+\infty} d\sigma \varrho(y_1, \sigma) \varrho(y_2, \sigma) p(\sigma). \quad (5)$$

Then, the two-particle rapidity correlation function is defined as

$$C_2(y_1, y_2) = \varrho_{\text{meas},2}(y_1, y_2) - \varrho_{\text{meas}}(y_1) \varrho_{\text{meas}}(y_2). \quad (6)$$

The second factorial cumulant is obtained by integrating the correlation function,

$$\hat{C}_2 = \int_{-Y}^Y dy_1 \int_{-Y}^Y dy_2 C_2(y_1, y_2), \quad (7)$$

where Y characterizes the rapidity range of the measured correlations.

By analogy, the averaged n -particle rapidity density distribution is

$$\begin{aligned} \varrho_{\text{meas},n}(y_1, y_2, \dots, y_n) \\ = \int_0^{+\infty} d\sigma \varrho(y_1, \sigma) \varrho(y_2, \sigma) \dots \varrho(y_n, \sigma) p(\sigma). \end{aligned} \quad (8)$$

For example, the three-particle correlation function reads

$$\begin{aligned} C_3(y_1, y_2, y_3) = & \varrho_{\text{meas},3}(y_1, y_2, y_3) - \varrho_{\text{meas}}(y_1) \varrho_{\text{meas}}(y_2) \\ & \times \varrho_{\text{meas}}(y_3) - \varrho_{\text{meas}}(y_1) C_2(y_2, y_3) \\ & - \varrho_{\text{meas}}(y_2) C_2(y_1, y_3) - \varrho_{\text{meas}}(y_3) C_2(y_1, y_2), \end{aligned} \quad (9)$$

and n -particle correlation functions ($n = 4, 5, 6$) are defined, e.g., in Ref. [27]. The n th factorial cumulant is obtained by

$$\hat{C}_n = \int_{-Y}^Y dy_1 \dots \int_{-Y}^Y dy_n C_n(y_1, y_2, \dots, y_n). \quad (10)$$

A. Correlation functions and factorial cumulants for the quadratic rapidity distribution

In our calculations, we assume the quadratic single-particle rapidity density distribution (2) which is a good approximation in the midrapidity region. It is convenient to introduce the notation

$$m_k = \left\langle \frac{1}{\sigma^k} \right\rangle = \int_0^{+\infty} d\sigma \frac{p(\sigma)}{\sigma^k}. \quad (11)$$

The σ averaged rapidity distribution (4) reads

$$Q_{\text{meas}}(y) = \frac{N_f}{\sqrt{2\pi}} \left(m_1 - \frac{1}{2} m_3 y^2 \right). \quad (12)$$

The first factorial cumulant (equal to the mean number of particles in the integration interval) is given by

$$\hat{C}_1 = \langle N \rangle = \int_{-Y}^Y dy Q_{\text{meas}}(y) = \frac{N_f Y}{\sqrt{2\pi}} \left(2m_1 - \frac{1}{3} m_3 Y^2 \right). \quad (13)$$

The two-particle rapidity density distribution, two-particle correlation function, and the second factorial cumulant

read

$$Q_{\text{meas},2}(y_1, y_2) = \left(\frac{N_f}{\sqrt{2\pi}} \right)^2 \left[m_2 - \frac{1}{2} m_4 (y_1^2 + y_2^2) + \frac{1}{4} m_6 y_1^2 y_2^2 \right], \quad (14)$$

$$C_2(y_1, y_2) = \left(\frac{N_f}{\sqrt{2\pi}} \right)^2 \frac{1}{2^2} \left[4A_{2,0} - 2A_{2,1}(y_1^2 + y_2^2) + A_{2,2} y_1^2 y_2^2 \right], \quad (15)$$

$$\hat{C}_2 = \left(\frac{N_f Y}{\sqrt{2\pi}} \right)^2 \left[4A_{2,0} - \frac{4}{3} A_{2,1} Y^2 + \frac{1}{9} A_{2,2} Y^4 \right], \quad (16)$$

where

$$A_{2,0} = m_2 - m_1^2, \quad A_{2,1} = m_4 - m_1 m_3, \quad A_{2,2} = m_6 - m_3^2. \quad (17)$$

The three-particle rapidity density distribution, correlation function, and the third factorial cumulant read

$$Q_{\text{meas},3}(y_1, y_2, y_3) = \left(\frac{N_f}{\sqrt{2\pi}} \right)^3 \left[m_3 - \frac{1}{2} m_5 (y_1^2 + y_2^2 + y_3^2) + \frac{1}{4} m_7 (y_1^2 y_2^2 + y_1^2 y_3^2 + y_2^2 y_3^2) - \frac{1}{8} m_9 y_1^2 y_2^2 y_3^2 \right], \quad (18)$$

$$C_3(y_1, y_2, y_3) = \left(\frac{N_f}{\sqrt{2\pi}} \right)^3 \frac{1}{2^3} \left[8A_{3,0} - 4A_{3,1}(y_1^2 + y_2^2 + y_3^2) + 2A_{3,2}(y_1^2 y_2^2 + y_1^2 y_3^2 + y_2^2 y_3^2) - A_{3,3} y_1^2 y_2^2 y_3^2 \right], \quad (19)$$

$$\hat{C}_3 = \left(\frac{N_f Y}{\sqrt{2\pi}} \right)^3 \left[8A_{3,0} - 4A_{3,1} Y^2 + \frac{2}{3} A_{3,2} Y^4 - \frac{1}{27} A_{3,3} Y^6 \right], \quad (20)$$

where

$$\begin{aligned} A_{3,0} &= 2m_3^3 - 3m_1 m_2 + m_3, & A_{3,1} &= 2m_1^2 m_3 - m_2 m_3 - 2m_1 m_4 + m_5, \\ A_{3,2} &= 2m_1 m_3^2 - 2m_3 m_4 - m_1 m_6 + m_7, & A_{3,3} &= 2m_3^3 - 3m_3 m_6 + m_9. \end{aligned} \quad (21)$$

The four-particle rapidity density distribution is given by

$$Q_{\text{meas},4}(y_1, y_2, y_3, y_4) = \left(\frac{N_f}{\sqrt{2\pi}} \right)^4 \left[m_4 - \frac{1}{2} m_6 \sum_{i=1}^4 y_i^2 + \frac{1}{4} m_8 \sum_{j>i} y_i^2 y_j^2 - \frac{1}{8} m_{10} \sum_{k>j>i} y_i^2 y_j^2 y_k^2 + \frac{1}{16} m_{12} y_1^2 y_2^2 y_3^2 y_4^2 \right]. \quad (22)$$

The four-particle correlation function and the fourth factorial cumulant read

$$C_4(y_1, y_2, y_3, y_4) = \left(\frac{N_f}{\sqrt{2\pi}} \right)^4 \frac{1}{2^4} \left[-16A_{4,0} + 8A_{4,1} \sum_{i=1}^4 y_i^2 - 4A_{4,2} \sum_{j>i} y_i^2 y_j^2 - 2A_{4,3} \sum_{k>j>i} y_i^2 y_j^2 y_k^2 + A_{4,4} y_1^2 y_2^2 y_3^2 y_4^2 \right], \quad (23)$$

$$\hat{C}_4 = \left(\frac{N_f Y}{\sqrt{2\pi}} \right)^4 \left[-16A_{4,0} + \frac{32}{3} A_{4,1} Y^2 - \frac{8}{3} A_{4,2} Y^4 - \frac{8}{27} A_{4,3} Y^6 + \frac{1}{81} A_{4,4} Y^8 \right], \quad (24)$$

where

$$\begin{aligned} A_{4,0} &= 6m_1^4 - 12m_1^2 m_2 + 3m_2^2 + 4m_1 m_3 - m_4, \\ A_{4,1} &= 6m_1^3 m_3 - 6m_1 m_2 m_3 + m_3^2 - 6m_1^2 m_4 + 3m_2 m_4 \\ &\quad + 3m_1 m_5 - m_6, \\ A_{4,2} &= 6m_1^2 m_3^2 - 2m_2 m_3^2 - 8m_1 m_3 m_4 + 2m_4^2 + 2m_3 m_5 \\ &\quad - 2m_1^2 m_6 + m_2 m_6 + 2m_1 m_7 - m_8, \end{aligned}$$

$$\begin{aligned} A_{4,3} &= m_{10} - 6m_1 m_3^3 + 6m_3^2 m_4 + 6m_1 m_3 m_6 - 3m_4 m_6 \\ &\quad - 3m_3 m_7 - m_1 m_9, \\ A_{4,4} &= m_{12} - 6m_3^4 + 12m_3^2 m_6 - 3m_6^2 - 4m_3 m_9. \end{aligned} \quad (25)$$

Five- and six-particle correlation functions and the corresponding factorial cumulants are presented in the Appendix.

We note that \hat{C}_k is proportional to N_f^k which indicates the long-range correlations. This is understandable since the

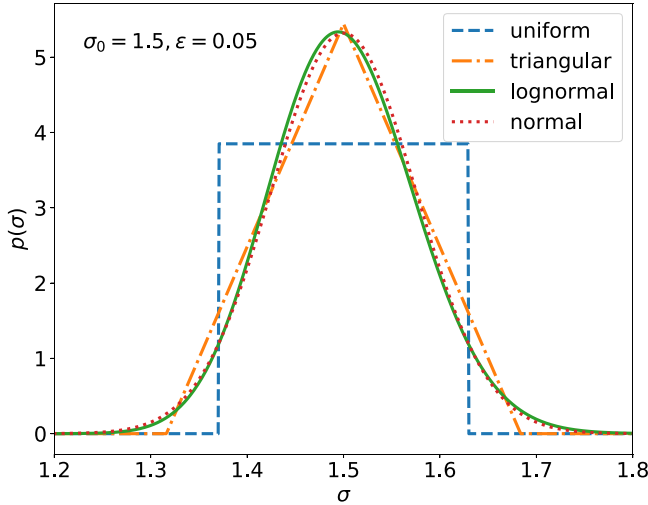


FIG. 2. Different σ distributions studied in this paper. They all have the same expectation σ_0 and the standard deviation $\varepsilon\sigma_0$.

change of the width of the distribution modifies the distribution in the whole rapidity range.

B. σ fluctuations

We do not know how σ fluctuates in realistic heavy-ion collisions however we may study various probability distributions $p(\sigma)$ to obtain a better insight. In all the presented distributions we require that

$$\langle \sigma \rangle = \sigma_0 \quad (26)$$

and the standard deviation

$$\sqrt{\langle (\sigma - \langle \sigma \rangle)^2 \rangle} = \varepsilon\sigma_0, \quad (27)$$

where ε can vary and determines the strength of the σ fluctuations. For $\varepsilon = 0$, there are no σ fluctuations and all the correlations vanish. Various σ distributions with σ_0 , and ε used in our calculations are presented in Fig. 2.

1. Uniform distribution

First, we assume that σ follows a uniform distribution. It is the simplest distribution to study however most likely it is not very realistic. Namely,

$$p(\sigma) = \begin{cases} \frac{1}{2\sqrt{3}\varepsilon\sigma_0} & \text{if } \sigma \in [\sigma_0(1 - \sqrt{3}\varepsilon), \sigma_0(1 + \sqrt{3}\varepsilon)] \\ 0 & \text{otherwise,} \end{cases} \quad (28)$$

where we assume $0 \leq \varepsilon \leq \frac{1}{\sqrt{3}}$. The interval within which the distribution $p(\sigma)$ is nonzero is uniquely fixed by condition (27). We obtain¹

$$m_1 = \frac{1}{2\sqrt{3}\varepsilon\sigma_0} \ln \left(\frac{1 + \sqrt{3}\varepsilon}{1 - \sqrt{3}\varepsilon} \right),$$

¹We note that $m_1 = \lim_{k \rightarrow 1} m_k$.

$$m_k = \frac{1}{2\sqrt{3}\varepsilon\sigma_0^k} \frac{(1 - \sqrt{3}\varepsilon)^{1-k} - (1 + \sqrt{3}\varepsilon)^{1-k}}{k-1}, \quad (29)$$

$$k = 2, 3, \dots$$

One can calculate full analytic expressions for the factorial cumulants by applying Eqs. (29) to Eqs. (13), (16), (20), and (24). ε is expected to be small, so we can expand full expressions into power series in terms of ε about zero. Here we present the leading-order terms (lowest power in ε):

$$\hat{C}_1 \approx \frac{N_t z}{\sqrt{2\pi}} \left(2 - \frac{1}{3} z^2 \right), \quad (30)$$

$$\hat{C}_2 \approx \left(\frac{N_t z}{\sqrt{2\pi}} \right)^2 \varepsilon^2 (2 - z^2)^2, \quad (31)$$

$$\hat{C}_3 \approx \left(\frac{N_t z}{\sqrt{2\pi}} \right)^3 \frac{24\varepsilon^4}{5} (2 - z^2)^2 (1 - z^2), \quad (32)$$

$$\hat{C}_4 \approx - \left(\frac{N_t z}{\sqrt{2\pi}} \right)^4 \frac{6\varepsilon^4}{5} (2 - z^2)^4, \quad (33)$$

where

$$z = \frac{Y}{\sigma_0}. \quad (34)$$

The factorial cumulants \hat{C}_5 and \hat{C}_6 are presented in the Appendix.

2. Triangular distribution

A step towards a more realistic σ distribution is the triangular distribution. Namely,

$$p(\sigma) = \begin{cases} \frac{\sigma - \sigma_0(1 - \sqrt{6}\varepsilon)}{6\varepsilon^2\sigma_0^2} & \text{if } \sigma \in [\sigma_0(1 - \sqrt{6}\varepsilon), \sigma_0] \\ \frac{-\sigma + \sigma_0(1 + \sqrt{6}\varepsilon)}{6\varepsilon^2\sigma_0^2} & \text{if } \sigma \in (\sigma_0, \sigma_0(1 + \sqrt{6}\varepsilon)] \\ 0 & \text{otherwise,} \end{cases} \quad (35)$$

where $0 \leq \varepsilon \leq \frac{1}{\sqrt{6}}$, and the interval within which the distribution $p(\sigma)$ is nonzero is fixed by Eq. (27).

Then,²

$$m_1 = \frac{1}{6\varepsilon^2\sigma_0} [(1 + \sqrt{6}\varepsilon) \ln(1 + \sqrt{6}\varepsilon) + (1 - \sqrt{6}\varepsilon) \ln(1 - \sqrt{6}\varepsilon)],$$

$$m_2 = -\frac{1}{6\varepsilon^2\sigma_0^2} \ln(1 - 6\varepsilon^2),$$

$$m_k = \frac{1}{6\varepsilon^2\sigma_0^k (k-1)(k-2)} \times \left[\frac{1}{(1 - \sqrt{6}\varepsilon)^{k-2}} + \frac{1}{(1 + \sqrt{6}\varepsilon)^{k-2}} - 2 \right],$$

$$k = 3, 4, 5, \dots \quad (36)$$

²We note that $m_1 = \lim_{k \rightarrow 1} m_k$ and $m_2 = \lim_{k \rightarrow 2} m_k$.

One can calculate full analytic expressions for \hat{C}_k using Eqs. (13), (16), (20), and (24). The leading-order terms (low-order power in ε) are given by

$$\hat{C}_1 \approx \frac{N_t z}{\sqrt{2\pi}} \left(2 - \frac{1}{3} z^2 \right), \quad (37)$$

$$\hat{C}_2 \approx \left(\frac{N_t z}{\sqrt{2\pi}} \right)^2 \varepsilon^2 (2 - z^2)^2, \quad (38)$$

$$\hat{C}_3 \approx \left(\frac{N_t z}{\sqrt{2\pi}} \right)^3 \frac{42\varepsilon^4}{5} (2 - z^2)^2 (1 - z^2), \quad (39)$$

$$\hat{C}_4 \approx - \left(\frac{N_t z}{\sqrt{2\pi}} \right)^4 \frac{3\varepsilon^4}{5} (2 - z^2)^4, \quad (40)$$

where z is given by Eq. (34). The higher-order factorial cumulants are presented in the Appendix.

3. Lognormal distribution

It would be natural to assume that σ follows the normal distribution however, by definition $\sigma \geq 0$, whereas the normal distribution allows also for negative values. Also, the integrals used to calculate m_k , Eq. (11), do not converge for the normal distribution. To overcome these issues and still obtain analytic results, we assume that σ follows the lognormal distribution [its domain by definition is $(0, +\infty)$]. Namely,

$$p(\sigma) = \frac{1}{\sqrt{2\pi} b \sigma} \exp \left(- \frac{(\ln \sigma - a)^2}{2b^2} \right). \quad (41)$$

Its expectation $\langle \sigma \rangle = \exp(a + \frac{b^2}{2})$ and its variance $\text{Var}(\sigma) = [\exp(b^2) - 1] \exp(2a + b^2)$. This with the constraints (26) and (27) gives

$$a = \ln \left(\frac{\sigma_0}{\sqrt{\varepsilon^2 + 1}} \right), \quad b = \sqrt{\ln(\varepsilon^2 + 1)}. \quad (42)$$

We have checked that such a distribution is very close to the corresponding normal distribution, as can be seen in Fig. 2.

For this distribution,

$$m_k = \frac{(1 + \varepsilon^2)^{\frac{k(k+1)}{2}}}{\sigma_0^k} \quad \text{for } k = 1, 2, 3, \dots \quad (43)$$

Again, one can easily calculate the full analytic expressions for \hat{C}_k using Eqs. (13), (16), (20), and (24). For small ε , the leading-order terms read:

$$\hat{C}_1 \approx \frac{N_t z}{\sqrt{2\pi}} \left(2 - \frac{1}{3} z^2 \right), \quad (44)$$

$$\hat{C}_2 \approx \left(\frac{N_t z}{\sqrt{2\pi}} \right)^2 \varepsilon^2 (2 - z^2)^2, \quad (45)$$

$$\hat{C}_3 \approx \left(\frac{N_t z}{\sqrt{2\pi}} \right)^3 3\varepsilon^4 (2 - z^2)^2 (2 - 3z^2), \quad (46)$$

$$\hat{C}_4 \approx \left(\frac{N_t z}{\sqrt{2\pi}} \right)^4 16\varepsilon^6 (2 - z^2)^2 (9z^4 - 14z^2 + 4), \quad (47)$$

where z is given by Eq. (34). The higher-order factorial cumulants are presented in the Appendix.

We note that for all three studied distributions, the factorial cumulants depend on $z = Y/\sigma_0$ and not on Y and σ_0 separately. The leading-order term of \hat{C}_k is always proportional to $(N_t z)^k$. As expected, when $\varepsilon \rightarrow 0$, all $\hat{C}_k = 0$ ($k \geq 2$) because in this case there are no width fluctuations. We also note that the leading-order terms of \hat{C}_1 and \hat{C}_2 are the same for the three studied $p(\sigma)$ distributions. It can be shown that this is the case for all possible $p(\sigma)$ distributions satisfying Eqs. (26) and (27), whereas the higher-order terms and exact results differ among the distributions.³

4. Truncated normal distribution—numerical computations

Here we assume that σ follows the normal distribution given by

$$p(\sigma) = \frac{1}{\sqrt{2\pi} \varepsilon \sigma_0} \exp \left(- \frac{(\sigma - \sigma_0)^2}{2(\varepsilon \sigma_0)^2} \right), \quad (48)$$

where, as in uniform, triangular, and lognormal distributions, we require the expectation to be σ_0 and the standard deviation $\varepsilon \sigma_0$. To require $\sigma > 0$ we use the truncated normal distribution.⁴ As mentioned earlier, we were unable to obtain analytic results for the normal distribution however we calculated m_k numerically using [34]. To test this approach, we used the same numerical method for uniform, triangular, and lognormal distributions and reproduced the exact results with great precision.

III. CUMULANT RATIOS

Here we show the cumulant ratios extracted from the factorial cumulants obtained for the quadratic rapidity density distribution (2). We use the relations between the cumulants and factorial cumulants [35].⁵

Our assumption of the Gaussian (approximately quadratic) proton rapidity density distribution is applicable for low collision energies where also the interesting anomalies of the

³The fact that the leading-order terms of \hat{C}_1 and \hat{C}_2 are independent of σ distribution can be justified by expanding m_k into series. Namely,

$$m_k = \frac{1}{\sigma_0^k} \int d\sigma \frac{p(\sigma)}{(1+x)^k},$$

where $x = (\sigma - \sigma_0)/\sigma_0$ is assumed to be small. Expanding $\frac{1}{(1+x)^k}$ into a series about zero, one obtains m_k as an infinite series in terms of $s_k = \mu_k/\sigma_0^k$, where $\mu_k = \langle (\sigma - \sigma_0)^k \rangle$ is the k th central moment of σ distribution. $s_1 = 0$ and $s_2 = \varepsilon^2$ for all the σ distributions that satisfy Eqs. (26) and (27). We note that, for $k \geq 3$, s_k is distribution dependent and such terms do not appear in the leading-order terms of \hat{C}_1 and \hat{C}_2 .

⁴We use the truncated, normalized normal distribution, $\tilde{p}(\sigma) = Ap(\sigma)$ if $\sigma \in [a, b]$ and $\tilde{p}(\sigma) = 0$ otherwise, where $p(\sigma)$ is given by Eq. (48) and $A = 1/\int_a^b d\sigma p(\sigma)$ with a and b being the limits of the σ interval.

⁵See also Appendix A of Ref. [8] for explicit formulas for the first six cumulants.

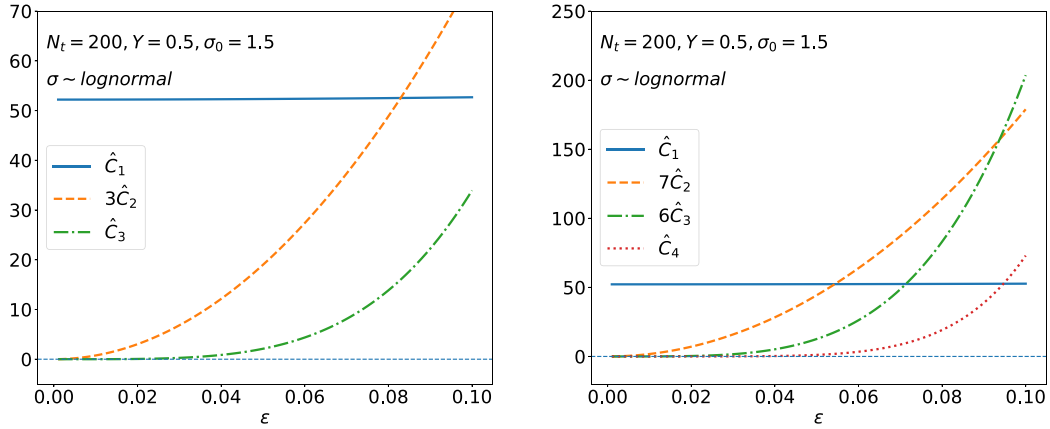


FIG. 3. The contributions of different-order factorial cumulants \hat{C}_k to cumulants, κ_3 (left) and κ_4 (right). They are calculated from the quadratic proton rapidity density distribution (2) with σ following lognormal distribution (41) using exact analytic results from Eqs. (13), (16), (20), (24). The coefficients in front of \hat{C}_k originate from the relation between cumulants and factorial cumulants, namely $\kappa_3 = \hat{C}_1 + 3\hat{C}_2 + \hat{C}_3$ and $\kappa_4 = \hat{C}_1 + 7\hat{C}_2 + 6\hat{C}_3 + \hat{C}_4$. The values of N_t , Y , and σ_0 roughly correspond to the STAR measurements in central Au + Au collisions at 7.7 GeV.

scaled kurtosis were measured by the STAR Collaboration [36]. We have used the simulated net-proton rapidity density distribution in central 0%–5% Au + Au collisions at $\sqrt{s_{NN}} = 7.7$ GeV from Ref. [37] to roughly estimate that $N_t \approx 200$ and $\sigma_0 \approx 1.5$ are reasonable values.⁶ For $\sqrt{s_{NN}} = 3$ GeV, we have used the preliminary STAR data on proton density distribution in central 0%–5% Au + Au collisions [33] and extracted the parameters $N_t \approx 175$, $\sigma_0 \approx 0.75$. We note that the estimated $\sigma_0(3 \text{ GeV})/\sigma_0(7.7 \text{ GeV}) = 0.75/1.5 = 0.5$ is very close to the rough estimate $\ln(3)/\ln(7.7) \approx 0.54$.⁷ We choose $Y = 0.5$ as in the STAR measurements.

In our calculations we have tried two methods of approximating the cumulant ratios. In the first method, we calculate the cumulants from the factorial cumulants using only the earlier presented leading-order terms of \hat{C}_n . This approximation works very well in most of the cases as seen in the following examples. The results of this method are denoted in the figures as “approx with \hat{C} .”

In the second method, we calculate the cumulants from the factorial cumulants using exact expressions for \hat{C}_n and then we approximate the obtained cumulant ratios by the power series expansion about $\varepsilon = 0$. We obtain the expansions of the form

$$\frac{\kappa_n}{\kappa_2} = 1 + a_n f(N_t, z) \varepsilon^2 + \underbrace{\dots}_{O(\varepsilon^4)}, \quad (49)$$

⁶At low energies, there are very few produced antiprotons. Therefore, the net-proton rapidity density distribution is a good approximation of the proton distribution. As mentioned earlier, treating the single-particle rapidity distribution as a single Gaussian or quadratic function is only a rough approximation.

⁷The width of the single-particle rapidity density distribution roughly scales as $\ln(\sqrt{s_{NN}})$.

where $a_n = 6, 18, 42, 90$ for $n = 3, 4, 5, 6$, respectively,

$$f(N_t, z) = \frac{N_t z}{\sqrt{2\pi}} \frac{(2 - z^2)^2}{6 - z^2} \quad (50)$$

is universal for studied σ distributions (uniform, triangular, lognormal) and various orders of cumulants, whereas higher-order terms differ between the distributions and orders of cumulants. The same expansion is also obtained for κ_2/κ_1 with the coefficient equal to three. We show the result of this method as “approx with κ up to ε^2 .” As seen from the following examples, this approximation works well for small ε .⁸ Therefore, for small σ fluctuations, each of the studied cumulant ratios is described by the common formula for very different σ distributions. This suggests that the cumulant ratios are independent of $p(\sigma)$ for small ε . $f(N_t, z)$ is found to be equivalent to considering only the leading-order terms of \hat{C}_1 and \hat{C}_2 and neglecting higher-order factorial cumulants. This indicates that, for small ε , the cumulant ratios are dominated by two-particle correlations. This is further supported by Fig. 3.

A. $\sqrt{s_{NN}} = 7.7$ GeV

We assume $N_t = 200$, $\sigma_0 = 1.5$, $Y = 0.5$ which roughly correspond to the STAR measurements in central Au + Au collisions at $\sqrt{s_{NN}} = 7.7$ GeV.

In Fig. 4, we show exact κ_2/κ_1 (calculated with all $A_{i,j}$) for σ following the uniform, triangular, and lognormal distributions. We note that the scaled variance is very similar for all three $p(\sigma)$. For the lognormal distribution we show also the

⁸We have checked that including ε^4 terms improves the results but works worse than the “approx. with \hat{C} ” method.

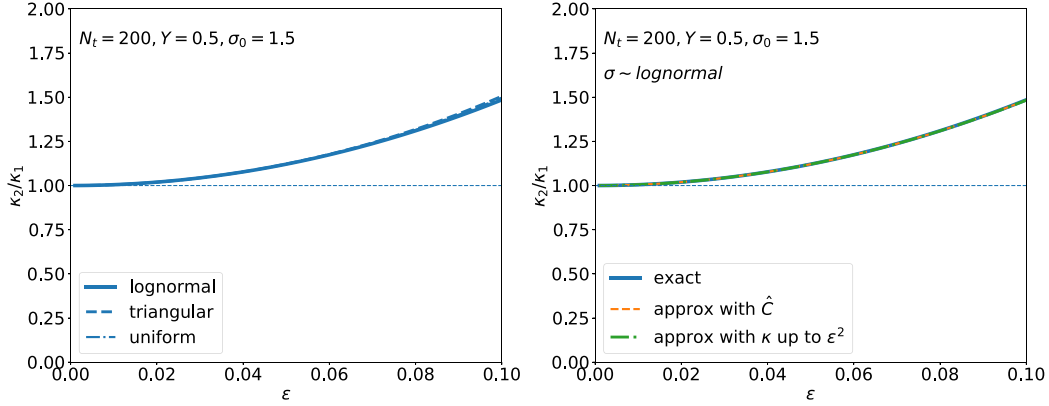


FIG. 4. (left) Scaled variance κ_2/κ_1 calculated from the quadratic proton rapidity density distribution (2) with σ following uniform (28), triangular (35), and lognormal distribution (41) using the exact analytic result from Eqs. (13) and (16). All three distributions give virtually the same results. (right) κ_2/κ_1 calculated using σ following lognormal distribution (41). Both approximations reproduce the exact results very well. The values of N_t , Y , and σ_0 roughly correspond to the STAR measurements in central Au + Au collisions at 7.7 GeV.

approximated results which are very close to the exact curve (the same is true for the uniform and triangular distributions). The cumulant ratios κ_3/κ_2 and κ_4/κ_2 with σ following the uniform distribution are presented in the first row, the results with triangular distribution are in the second row, whereas the results with lognormal distribution are in the third row of Fig. 5. The exact curves use the analytic exact results with all $A_{i,j}$ terms of the factorial cumulants. The dashed line $\kappa_n/\kappa_m = 1$ is the Poisson baseline for no correlations case. The cumulant ratios κ_5/κ_2 and κ_6/κ_2 are presented in the Appendix.

In the case of the truncated normal distribution, we calculate the factorial cumulants with $N_t = 200$, $Y = 0.5$, $\sigma_0 = 1.5$ using numerical integration for m_k (see previous section). The integration is done for $\epsilon \in [0.01, 3]$.⁹

In Fig. 6, we show the numerical results for the truncated normal distribution in comparison to the exact results with the lognormal distribution. The normal distribution results are in agreement with lognormal results for small ϵ , and for larger ϵ they follow the same trend though they give greater values.

B. $\sqrt{s_{NN}} = 3$ GeV

We note that the cumulant ratios at $\sqrt{s_{NN}} = 3$ GeV are measured by the STAR Collaboration in the asymmetric rapidity range, $y \in [-0.5, 0]$, whereas, at other collision energies, they are obtained within the symmetric interval, $y \in [-0.5, 0.5]$ [36]. As seen from Eqs. (12), (15), (19), and (23), the rapidity density distributions, as well as rapidity correlation functions are the even functions with respect to every y_i . Clearly, for any

function f satisfying this condition,

$$\begin{aligned} & \int_{-Y}^Y dy_1 \cdots \int_{-Y}^Y dy_n f(y_1, y_2, \dots, y_n) \\ &= 2^n \int_{-Y}^0 dy_1 \cdots \int_{-Y}^0 dy_n f(y_1, y_2, \dots, y_n). \end{aligned} \quad (51)$$

Therefore, the k th factorial cumulant from the rapidity correlation function in $[-Y, 0]$ is 2^k times smaller than the corresponding factorial cumulant in $[-Y, Y]$. Since the cumulants are the linear combinations of the factorial cumulants of a different order [35], the cumulant ratios are modified in a more complicated way.

Using $N_t = 175$ and $\sigma_0 = 0.75$ extracted from the fit to the STAR data at $\sqrt{s_{NN}} = 3$ GeV [33] and taking Eq. (51) into account, we have calculated the cumulant ratios, originating from the width fluctuations, in $y \in [-0.5, 0]$ as well as $y \in [-0.5, 0.5]$. They are presented in Figs. 7 and 8 for various σ distributions. The higher-order cumulant ratios are shown in the Appendix. We note that the results obtained in symmetric and asymmetric rapidity intervals differ significantly. We have checked that the previously discussed two methods of approximation also work but in Eq. (49) a_n should be divided by two.

IV. DISCUSSION AND SUMMARY

In this paper, we have presented the method of analytical calculation of the correlation functions, factorial cumulants, and cumulants originating from the fluctuating width of the proton rapidity density distribution. We have assumed that this distribution is a Gaussian function that can be approximated by the quadratic function in the midrapidity region. This assumption is valid for central low-energy Au + Au collisions. At higher energies (already slightly below 10 GeV), the distribution has a bimodal shape. The aim of our paper is to estimate the significance of the effect of width

⁹We have verified that both making this interval wider ($\sigma \in [0.005, 5]$) or more narrow ($\sigma \in [0.9, 2.1]$) does not change the cumulant ratios κ_3/κ_2 and κ_4/κ_2 for $\epsilon \in [0.01, 0.09]$. We have checked that the normalization constant is very close to 1 in all these intervals.

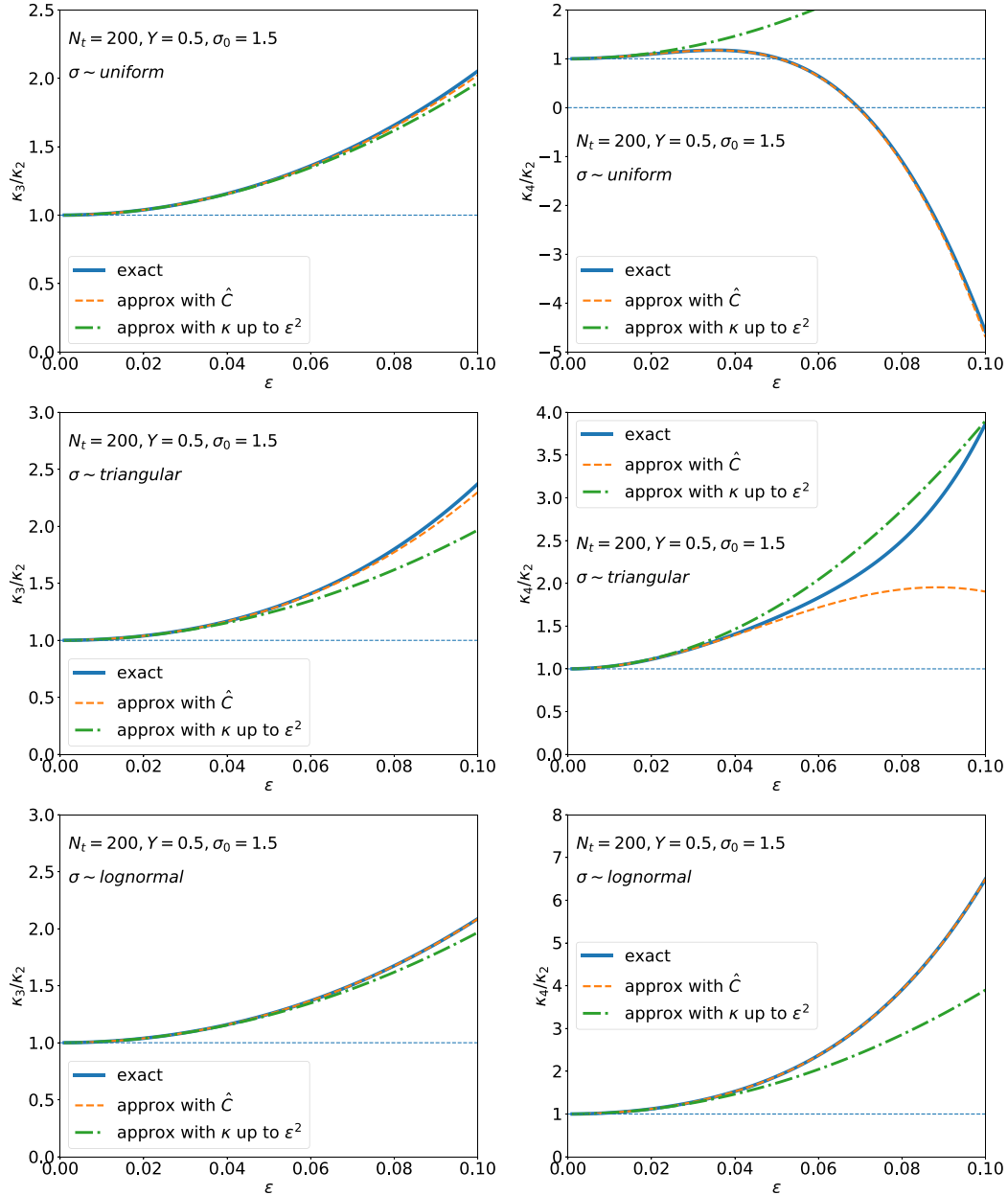


FIG. 5. The cumulant ratios, κ_3/κ_2 and κ_4/κ_2 , calculated from the quadratic proton rapidity density distribution (2) with σ following uniform distribution (28) (first row), triangular distribution (35) (second row), and lognormal distribution (41) (third row). “exact” is the exact analytic result from Eqs. (13), (16), (20), (24), with m_k given by Eq. (29), (36), and (43), respectively. “approx with \hat{C} ” is the result using the leading-order terms in ε for the factorial cumulants (see main text). “approx with κ up to ε^2 ” is the approximation using Eq. (49). The values of N_t , Y , and σ_0 roughly correspond to the STAR measurements in central Au + Au collisions at 7.7 GeV.

fluctuations rather than give precise results. We have studied the width σ fluctuations following three qualitatively different distributions, uniform, triangular, and lognormal (which approximates normal distribution). Obviously, they do not exhaust all the possibilities but we believe they constitute a representative choice.

We find that for very different σ distributions, all the cumulant ratios can be approximated by the universal function

(49) for small ε , where ε determines the strength of the σ fluctuations, see Eq. (27). This indicates that the results are independent of a choice of $p(\sigma)$ when the width fluctuations are small. This approximation is equivalent to considering only the leading-order terms of the first and second factorial cumulants which indeed are the same for any σ distribution with the same mean and standard deviation. Hence, at small ε , the cumulant ratios are governed by the two-particle correlations.

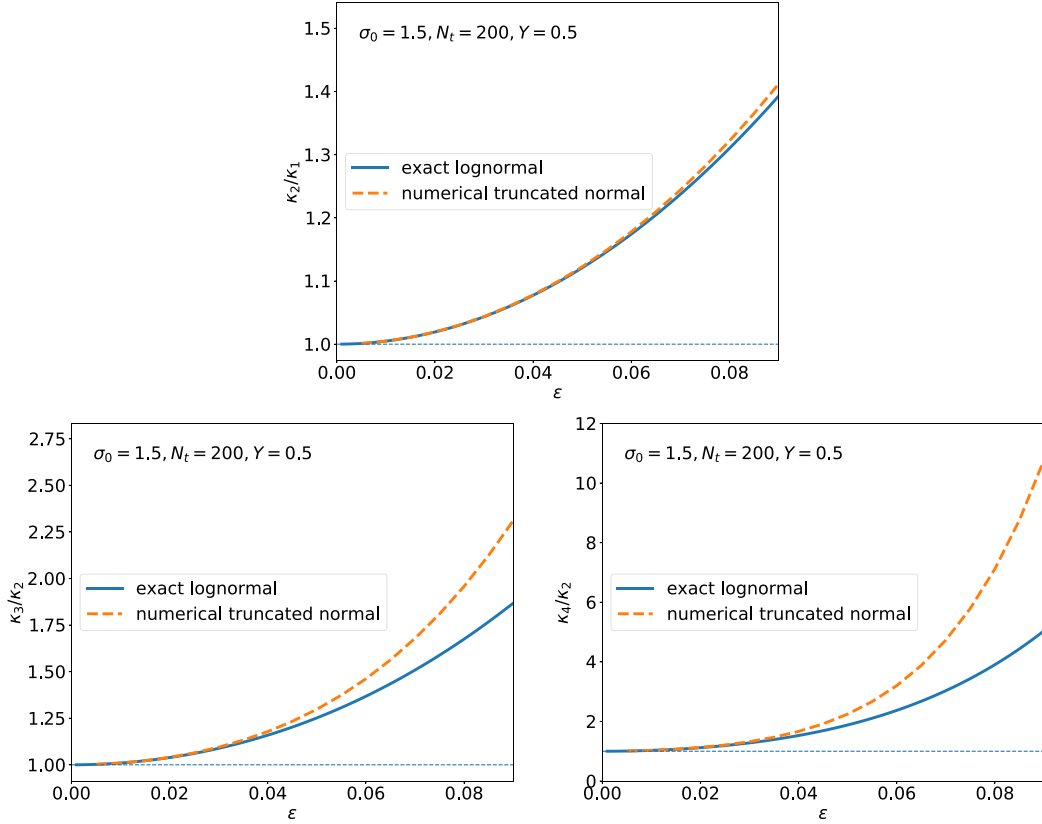


FIG. 6. The cumulant ratios, κ_2/κ_1 , κ_3/κ_2 , and κ_4/κ_2 calculated from the quadratic proton rapidity density distribution (2). The solid line assumes σ fluctuations following lognormal distribution (same as in Figs. 4 and 5) whereas the dashed line corresponds to the truncated normal distribution with the m_k calculated numerically. The values of N_t , Y , and σ_0 roughly correspond to the STAR measurements in central Au + Au collisions at 7.7 GeV.

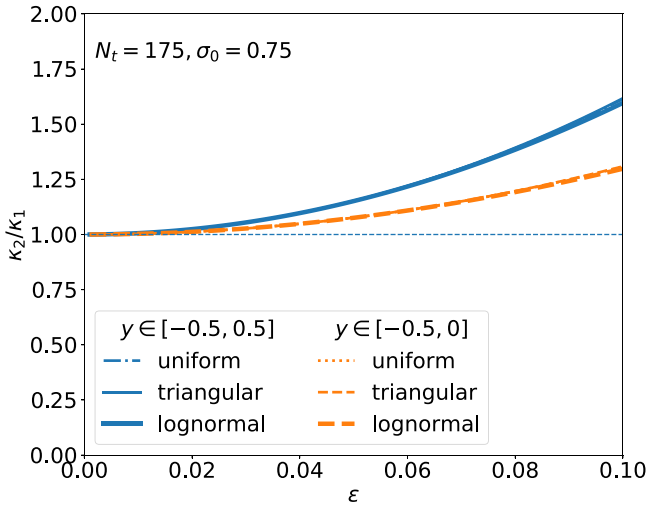


FIG. 7. The scaled variance κ_2/κ_1 calculated from the quadratic proton rapidity density distribution (2) with σ following uniform (28), triangular (35), and lognormal distribution (41), using exact formulas and values of N_t and σ_0 corresponding to central Au + Au collisions at 3 GeV. The results are compared for the wider ($y \in [-0.5, 0.5]$) and narrower ($y \in [-0.5, 0]$) rapidity range. For a given rapidity interval, all three distributions give very similar results.

In Table I, we present the STAR Collaboration data [38,39]. We note that the cumulant ratios from the width fluctuations for $\varepsilon < 0.05$ are of the same order of magnitude as measured experimentally. Hence, we have shown that the distribution width fluctuations due to fireball density fluctuations may have a measurable contribution to the cumulant ratios in heavy-ion experiments. Therefore, they should be further studied and taken into account in the search for the predicted first-order phase transition and critical point between the hadronic matter and quark-gluon plasma. A direct comparison with data is rather challenging because there are other sources of correlations, e.g., the global baryon number conservation [40–47]. It would be interesting to investigate the fluctuations in width of the rapidity distribution using various Monte Carlo models. The application of our method to the bimodal rapidity distribution (superposition of two Gaussians) would extend our results for much broader collision energy spectrum.

We have also demonstrated that the cumulant ratios measured in a symmetric and an asymmetric rapidity range might result in very different values. Therefore, one should be very careful when comparing the cumulant ratios measured in different rapidity intervals.

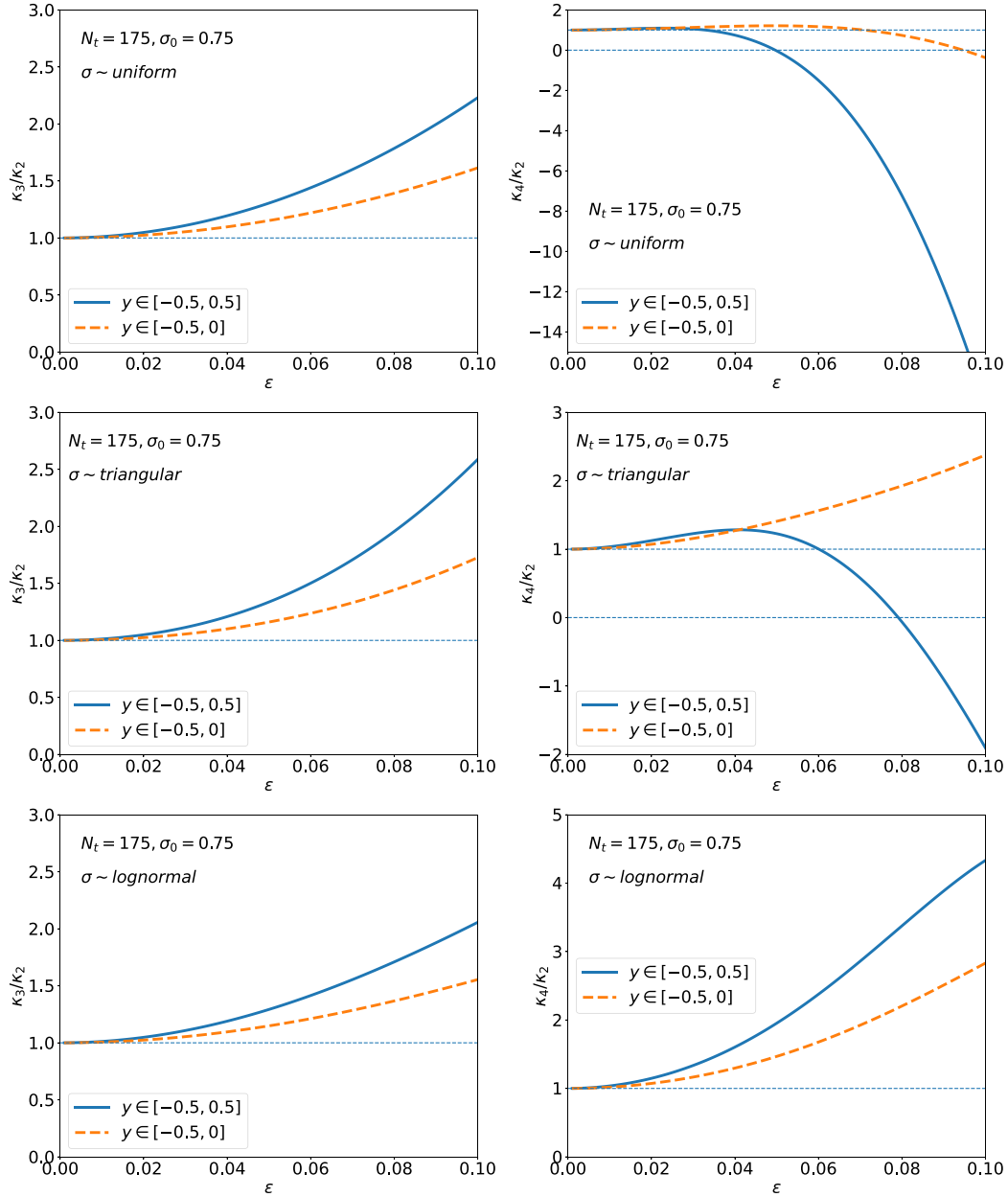


FIG. 8. The cumulant ratios κ_3/κ_2 and κ_4/κ_2 calculated from the quadratic proton rapidity density distribution (2) with σ following uniform (first row), triangular (second row), and lognormal (third row) distribution using exact formulas and values of N_t and σ_0 corresponding to central Au + Au collisions at 3 GeV. The results are compared for the wider ($y \in [-0.5, 0.5]$) and narrower ($y \in [-0.5, 0]$) rapidity range.

TABLE I. Cumulant ratios measured by the STAR Collaboration at the lowest energies [38,39].

$\sqrt{s_{NN}}$	3 GeV $y \in [-0.5, 0]$	7.7 GeV $y \in [-0.5, 0.5]$
κ_2/κ_1	$1.218 \pm 0.001(\text{stat.}) \pm 0.019(\text{syst.})$	$0.928 \pm 0.005(\text{stat.}) \pm 0.005(\text{syst.})$
κ_3/κ_2	$0.954 \pm 0.005(\text{stat.}) \pm 0.06(\text{syst.})$	$0.824 \pm 0.08(\text{stat.}) \pm 0.032(\text{syst.})$
κ_4/κ_2	$-0.85 \pm 0.09(\text{stat.}) \pm 0.80(\text{syst.})$	$1.8 \pm 1.2(\text{stat.}) \pm 0.4(\text{syst.})$

We note that the longitudinal fluctuations have already been studied by the expansion into orthogonal polynomials [4,27,28,30]. In this formalism, the width fluctuation is reflected in the second-order coefficient. In this paper, we have proposed another approach that focuses directly on the rapidity density distribution width fluctuations originating from the longitudinal fluctuations of the fireball density.

The goal of this work is to stimulate further research on longitudinal fluctuations. In principle, not only it can contribute to the important probes of a critical point such as the

proton multiplicity cumulants but also improve our understanding of the fireball longitudinal dynamics.

ACKNOWLEDGMENTS

We thank Volker Koch for useful discussions. This work was partially supported by the Ministry of Science and Higher Education (PL), and by the National Science Centre (PL), Grant No. 2018/30/Q/ST2/00101.

APPENDIX: THE HIGHER-ORDER CORRELATION FUNCTIONS AND FACTORIAL CUMULANTS

The subsequent n -particle rapidity density distributions follow the same pattern ($n = 5, 6$) as in Eqs. (14), (18), and (22). Namely,

$$\begin{aligned} Q_{\text{meas},5}(y_1, y_2, \dots, y_5) = & \left(\frac{N_t}{\sqrt{2\pi}} \right)^5 \left[m_5 - \frac{1}{2} m_7 \sum_{i=1}^5 y_i^2 + \frac{1}{4} m_9 \sum_{j>i} y_i^2 y_j^2 - \frac{1}{8} m_{11} \sum_{k>j>i} y_i^2 y_j^2 y_k^2 \right. \\ & \left. + \frac{1}{16} m_{13} \sum_{l>k>j>i} y_i^2 y_j^2 y_k^2 y_l^2 - \frac{1}{32} m_{15} y_1^2 y_2^2 \dots y_5^2 \right], \end{aligned} \quad (A1)$$

$$\begin{aligned} Q_{\text{meas},6}(y_1, y_2, \dots, y_6) = & \left(\frac{N_t}{\sqrt{2\pi}} \right)^6 \left[m_6 - \frac{1}{2} m_8 \sum_{i=1}^6 y_i^2 + \frac{1}{4} m_{10} \sum_{j>i} y_i^2 y_j^2 - \frac{1}{8} m_{12} \sum_{k>j>i} y_i^2 y_j^2 y_k^2 \right. \\ & \left. + \frac{1}{16} m_{14} \sum_{l>k>j>i} y_i^2 y_j^2 y_k^2 y_l^2 - \frac{1}{32} m_{16} \sum_{n>l>k>j>i} y_i^2 y_j^2 y_k^2 y_l^2 y_n^2 + \frac{1}{64} m_{18} y_1^2 y_2^2 \dots y_6^2 \right]. \end{aligned} \quad (A2)$$

The five-particle correlation function and the corresponding factorial cumulant read¹⁰

$$\begin{aligned} C_5(y_1, y_2, \dots, y_5) = & \left(\frac{N_t}{\sqrt{2\pi}} \right)^5 \frac{1}{2^5} \left[32A_{5,0} - 16A_{5,1} \sum_{i=1}^5 y_i^2 + 8A_{5,2} \sum_{j>i} y_i^2 y_j^2 - 4A_{5,3} \sum_{k>j>i} y_i^2 y_j^2 y_k^2 - 2A_{5,4} \sum_{l>k>j>i} y_i^2 y_j^2 y_k^2 y_l^2 \right. \\ & \left. - A_{5,5} y_1^2 y_2^2 y_3^2 y_4^2 y_5^2 \right], \end{aligned} \quad (A3)$$

$$\hat{C}_5 = \frac{N_t^5 Y^5}{(2\pi)^{5/2}} \left[32A_{5,0} - \frac{80}{3} A_{5,1} Y^2 + \frac{80}{9} A_{5,2} Y^4 - \frac{40}{27} A_{5,3} Y^6 - \frac{10}{81} A_{5,4} Y^8 - \frac{1}{243} A_{5,5} Y^{10} \right], \quad (A4)$$

where

$$\begin{aligned} A_{5,0} &= 24m_1^5 - 60m_1^3 m_2 + 30m_1 m_2^2 + 20m_1^2 m_3 - 10m_2 m_3 - 5m_1 m_4 + m_5, \\ A_{5,1} &= 24m_1^4 m_3 - 36m_1^2 m_2 m_3 + 6m_2^2 m_3 + 8m_1 m_3^2 - 24m_1^3 m_4 + 24m_1 m_2 m_4 - 5m_3 m_4 + 12m_1^2 m_5 \\ &\quad - 6m_2 m_5 - 4m_1 m_6 + m_7, \\ A_{5,2} &= 24m_1^3 m_3^2 - 18m_1 m_2 m_3^2 + 2m_3^3 - 36m_1^2 m_3 m_4 + 12m_2 m_3 m_4 + 12m_1 m_4^2 + 12m_1 m_3 m_5 \\ &\quad - 6m_4 m_5 - 6m_1^3 m_6 + 6m_1 m_2 m_6 - 3m_3 m_6 + 6m_1^2 m_7 - 3m_2 m_7 - 3m_1 m_8 + m_9, \\ A_{5,3} &= -2m_1 m_{10} + m_{11} + 24m_1^2 m_3^3 - 6m_2 m_3^3 - 36m_1 m_3^2 m_4 + 12m_3 m_4^2 + 6m_3^2 m_5 - 18m_1^2 m_3 m_6 \\ &\quad + 6m_2 m_3 m_6 + 12m_1 m_4 m_6 - 3m_5 m_6 + 12m_1 m_3 m_7 - 6m_4 m_7 - 3m_3 m_8 + 2m_1^2 m_9 - m_2 m_9, \\ A_{5,4} &= m_1 m_{12} - m_{13} + 4m_{10} m_3 - 24m_1 m_3^4 + 24m_3^3 m_4 + 36m_1 m_3^2 m_6 - 24m_3 m_4 m_6 - 6m_1 m_6^2 \\ &\quad - 12m_3^2 m_7 + 6m_6 m_7 - 8m_1 m_3 m_9 + 4m_4 m_9, \\ A_{5,5} &= m_{15} - 5m_{12} m_3 + 24m_3^5 - 60m_3^3 m_6 + 30m_3 m_6^2 + 20m_3^2 m_9 - 10m_6 m_9. \end{aligned} \quad (A5)$$

¹⁰They are calculated according to formulas given in Ref. [27].

The six-particle correlation function and the factorial cumulant are given by

$$C_6(y_1, y_2, \dots, y_6) = \left(\frac{N_t}{\sqrt{2\pi}} \right)^6 \frac{1}{2^6} \left[-64A_{6,0} + 32A_{6,1} \sum_{i=1}^6 y_i^2 + 16A_{6,2} \sum_{j>i} y_i^2 y_j^2 + 8A_{6,3} \sum_{k>j>i} y_i^2 y_j^2 y_k^2 \right. \\ \left. + 4A_{6,4} \sum_{l>k>j>i} y_i^2 y_j^2 y_k^2 y_l^2 + 2A_{6,5} \sum_{n>l>k>j>i} y_i^2 y_j^2 y_k^2 y_l^2 y_n^2 + A_{6,6} y_1^2 y_2^2 \cdots y_6^2 \right], \quad (\text{A6})$$

$$\hat{C}_6 = \frac{N_t^6 Y^6}{(2\pi)^3} \left[-64A_{6,0} + 64A_{6,1} Y^2 + \frac{80}{3} A_{6,2} Y^4 + \frac{160}{27} A_{6,3} Y^6 + \frac{20}{27} A_{6,4} Y^8 + \frac{4}{81} A_{6,5} Y^{10} + \frac{1}{729} A_{6,6} Y^{12} \right], \quad (\text{A7})$$

where

$$\begin{aligned} A_{6,0} &= 120m_1^6 - 360m_1^4 m_2 + 270m_1^2 m_2^2 - 30m_2^3 + 120m_1^3 m_3 - 120m_1 m_2 m_3 + 10m_3^2 - 30m_1^2 m_4 \\ &\quad + 15m_2 m_4 + 6m_1 m_5 - m_6, \\ A_{6,1} &= 120m_1^5 m_3 - 240m_1^3 m_2 m_3 + 90m_1 m_2^2 m_3 + 60m_1^2 m_3^2 - 20m_2 m_3^2 - 120m_1^4 m_4 + 180m_1^2 m_2 m_4 \\ &\quad - 30m_2^2 m_4 - 50m_1 m_3 m_4 + 5m_4^2 + 60m_1^3 m_5 - 60m_1 m_2 m_5 + 11m_3 m_5 - 20m_1^2 m_6 + 10m_2 m_6 + 5m_1 m_7 - m_8, \\ A_{6,2} &= m_{10} - 120m_1^4 m_3^2 + 144m_1^2 m_2 m_3^2 - 18m_2^2 m_3^2 - 24m_1 m_3^3 + 192m_1^3 m_3 m_4 - 144m_1 m_2 m_3 m_4 \\ &\quad + 18m_3^2 m_4 - 72m_1^2 m_4^2 + 24m_2 m_4^2 - 72m_1^2 m_3 m_5 + 24m_2 m_3 m_5 + 48m_1 m_4 m_5 - 6m_5^2 \\ &\quad + 24m_1^4 m_6 - 36m_1^2 m_2 m_6 + 6m_2^2 m_6 + 24m_1 m_3 m_6 - 9m_4 m_6 - 24m_1^3 m_7 + 24m_1 m_2 m_7 \\ &\quad - 6m_3 m_7 + 12m_1^2 m_8 - 6m_2 m_8 - 4m_1 m_9, \\ A_{6,3} &= -6m_1^2 m_{10} + 3m_1 m_{11} - m_{12} + 3m_{10} m_2 + 120m_1^3 m_3^3 - 72m_1 m_2 m_3^3 + 6m_3^4 - 216m_1^2 m_3^2 m_4 \\ &\quad + 54m_2 m_3^2 m_4 + 108m_1 m_3 m_4^2 - 12m_4^3 + 54m_1 m_3^2 m_5 - 36m_3 m_4 m_5 - 72m_1^3 m_3 m_6 \\ &\quad + 54m_1 m_2 m_3 m_6 - 12m_3^2 m_6 + 54m_1^2 m_4 m_6 - 18m_2 m_4 m_6 - 18m_1 m_5 m_6 + 3m_6^2 + 54m_1^2 m_3 m_7 \\ &\quad - 18m_2 m_3 m_7 - 36m_1 m_4 m_7 + 9m_5 m_7 - 18m_1 m_3 m_8 + 9m_4 m_8 + 6m_1^3 m_9 - 6m_1 m_2 m_9 + 4m_3 m_9, \\ A_{6,4} &= 2m_1^2 m_{12} - 2m_1 m_{13} + m_{14} - m_{12} m_2 + 16m_1 m_{10} m_3 - 4m_{11} m_3 - 120m_1^2 m_3^4 + 24m_2 m_3^4 \\ &\quad - 8m_{10} m_4 + 192m_1 m_3^3 m_4 - 72m_3^2 m_4^2 - 24m_3^3 m_5 + 144m_1^2 m_3^2 m_6 - 36m_2 m_3^2 m_6 \\ &\quad - 144m_1 m_3 m_4 m_6 + 24m_4^2 m_6 + 24m_3 m_5 m_6 - 18m_1^2 m_6^2 + 6m_2 m_6^2 - 72m_1 m_3^2 m_7 \\ &\quad + 48m_3 m_4 m_7 + 24m_1 m_6 m_7 - 6m_7^2 + 12m_3^2 m_8 - 6m_6 m_8 - 24m_1^2 m_3 m_9 + 8m_2 m_3 m_9 \\ &\quad + 16m_1 m_4 m_9 - 4m_5 m_9, \\ A_{6,5} &= m_1 m_{15} - m_{16} - 10m_1 m_{12} m_3 + 5m_{13} m_3 - 20m_{10} m_3^2 + 120m_1 m_3^5 + 5m_{12} m_4 - 120m_3^4 m_4 \\ &\quad + 10m_{10} m_6 - 240m_1 m_3^3 m_6 + 180m_3^2 m_4 m_6 + 90m_1 m_3 m_6^2 - 30m_4 m_6^2 + 60m_3^3 m_7 \\ &\quad - 60m_3 m_6 m_7 + 60m_1 m_3^2 m_9 - 40m_3 m_4 m_9 - 20m_1 m_6 m_9 + 10m_7 m_9, \\ A_{6,6} &= m_{18} - 6m_{15} m_3 + 30m_{12} m_3^2 - 120m_3^6 - 15m_{12} m_6 + 360m_3^4 m_6 - 270m_3^2 m_6^2 + 30m_6^3 \\ &\quad - 120m_3^3 m_9 + 120m_3 m_6 m_9 - 10m_9^2. \end{aligned} \quad (\text{A8})$$

In the case of the uniform σ distribution, Eq. (28), the approximated formulas (leading-order terms of the power series expansion about $\varepsilon = 0$) read

$$\hat{C}_5 \approx - \left(\frac{N_t z}{\sqrt{2\pi}} \right)^5 \frac{192\varepsilon^6}{7} (2 - z^2)^4 (1 - z^2), \quad (\text{A9})$$

$$\hat{C}_6 \approx \left(\frac{N_t z}{\sqrt{2\pi}} \right)^6 \frac{48\varepsilon^6}{7} (2 - z^2)^6. \quad (\text{A10})$$

For the triangular distribution, Eq. (35), we have

$$\hat{C}_5 \approx - \left(\frac{N_t z}{\sqrt{2\pi}} \right)^5 \frac{216\varepsilon^6}{7} (2 - z^2)^4 (1 - z^2), \quad (\text{A11})$$

$$\hat{C}_6 \approx \left(\frac{N_t z}{\sqrt{2\pi}} \right)^6 \frac{12\varepsilon^6}{7} (2 - z^2)^6. \quad (\text{A12})$$

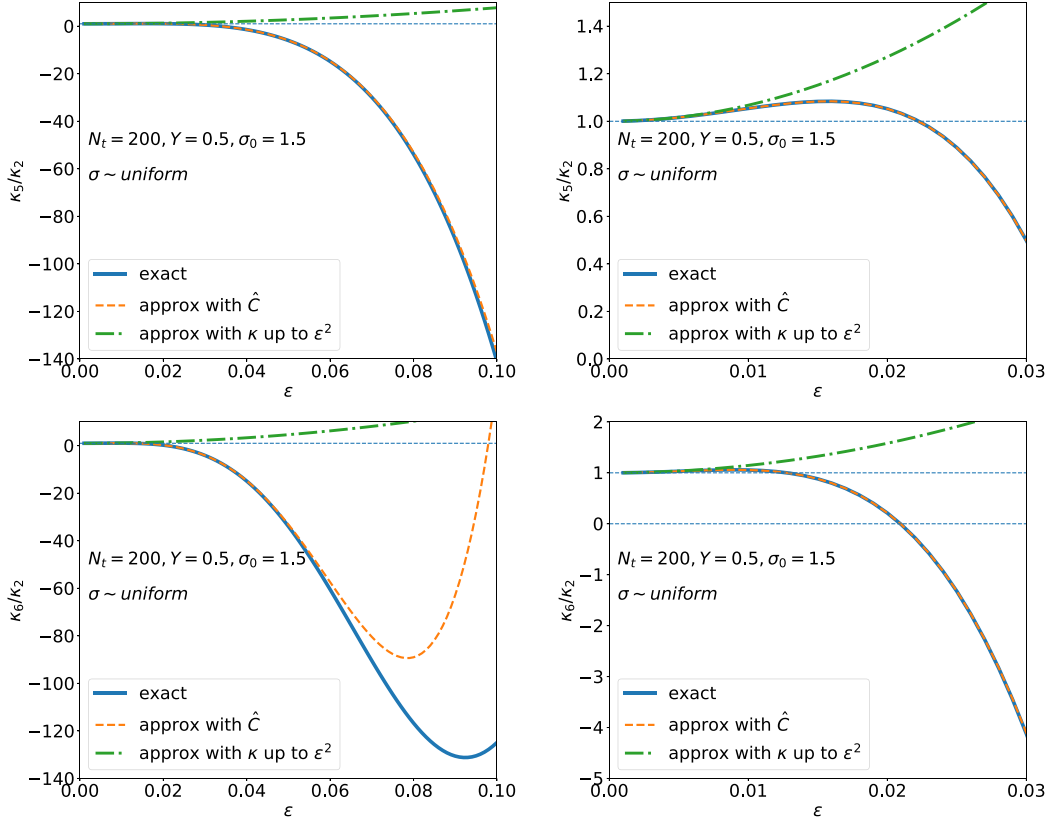


FIG. 9. κ_5/κ_2 and κ_6/κ_2 for σ following the uniform distribution. The left-hand side plots show a wider ε range $[0, 0.1]$ whereas the right-hand side plots show details at small $\varepsilon \in [0, 0.03]$.

For the lognormal distribution, Eq. (41), we obtain

$$\hat{C}_5 \approx \left(\frac{N_t z}{\sqrt{2\pi}} \right)^5 5\varepsilon^8 (2 - z^2)^2 (200 - 1172z^2 + 1694z^4 - 675z^6), \quad (\text{A13})$$

$$\hat{C}_6 \approx \left(\frac{N_t z}{\sqrt{2\pi}} \right)^6 48\varepsilon^{10} (2 - z^2)^2 (432 - 3664z^2 + 8728z^4 - 7636z^6 + 2187z^8). \quad (\text{A14})$$

The cumulant ratios, κ_5/κ_2 and κ_6/κ_2 , with σ following the uniform, triangular, and lognormal distributions are presented in Figs. 9–11.

In Figs. 12–14, we compare the cumulant ratios, κ_5/κ_2 and κ_6/κ_2 , obtained in the symmetric ($y \in [-0.5, 0.5]$) and asymmetric ($y \in [-0.5, 0]$) rapidity interval for all three analytically studied σ distributions with N_t and σ_0 corresponding to the STAR measurements at 3 GeV.

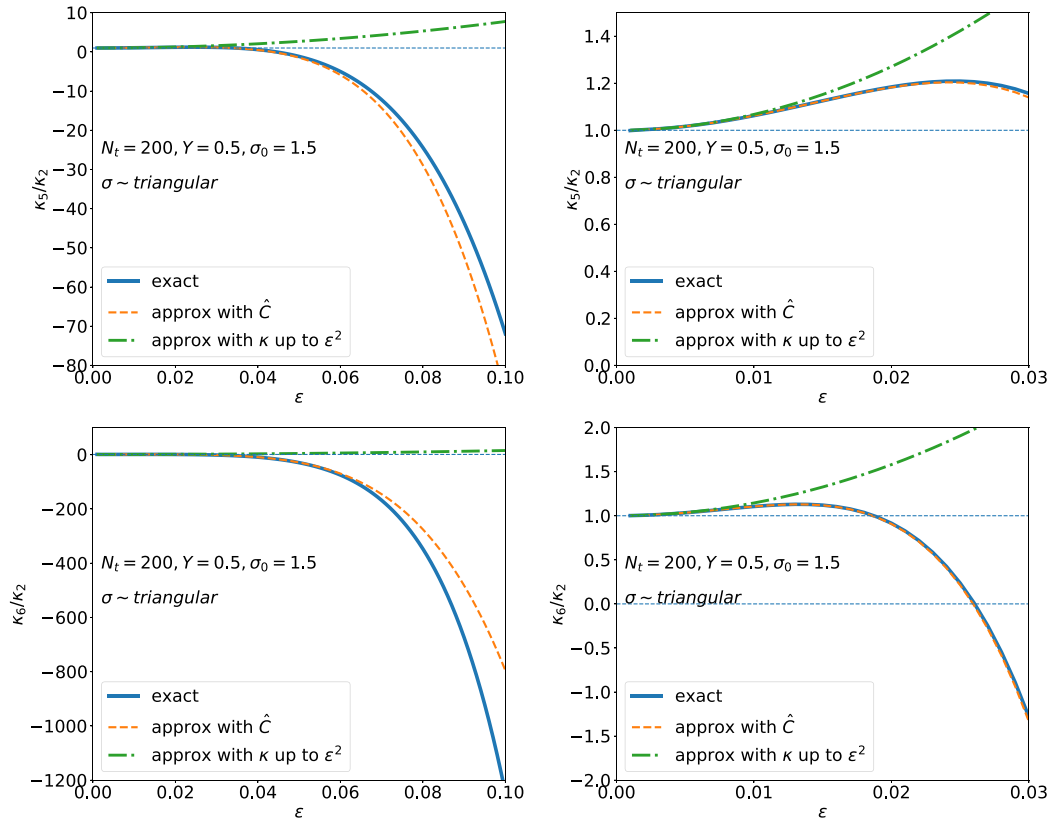


FIG. 10. Same as Fig. 9 but for σ following the triangular distribution.

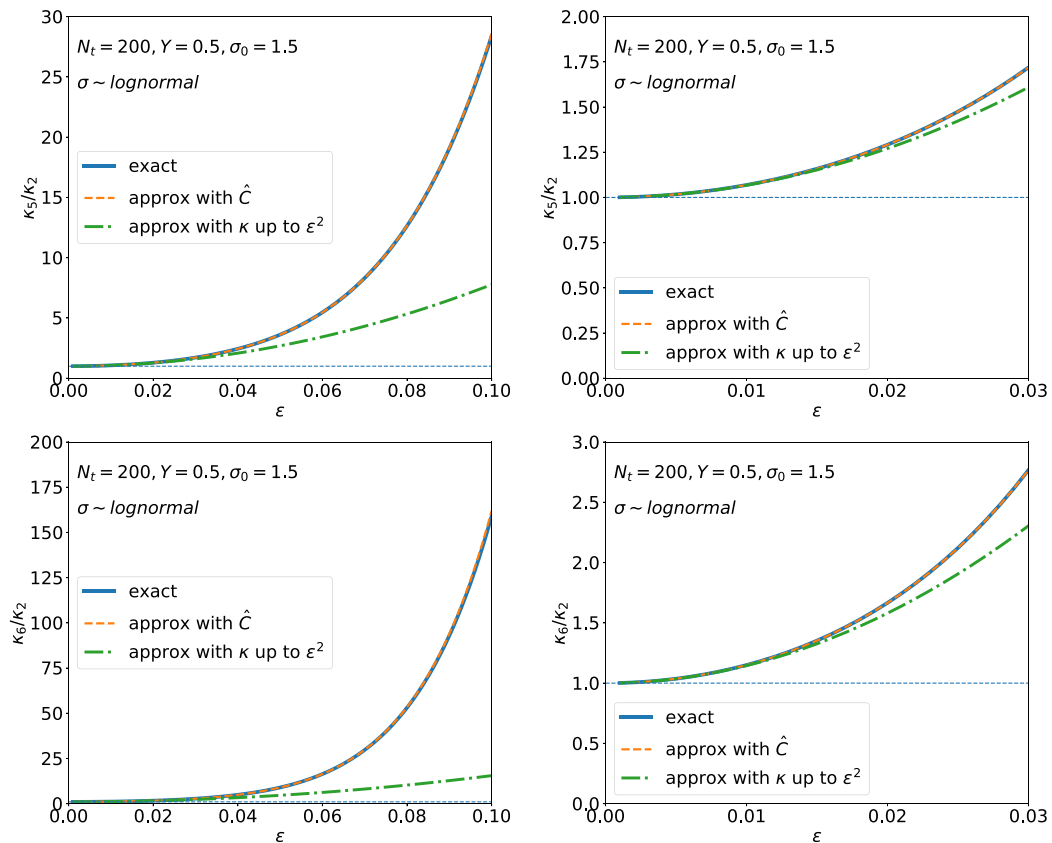


FIG. 11. Same as Fig. 9 but for σ following the lognormal distribution.

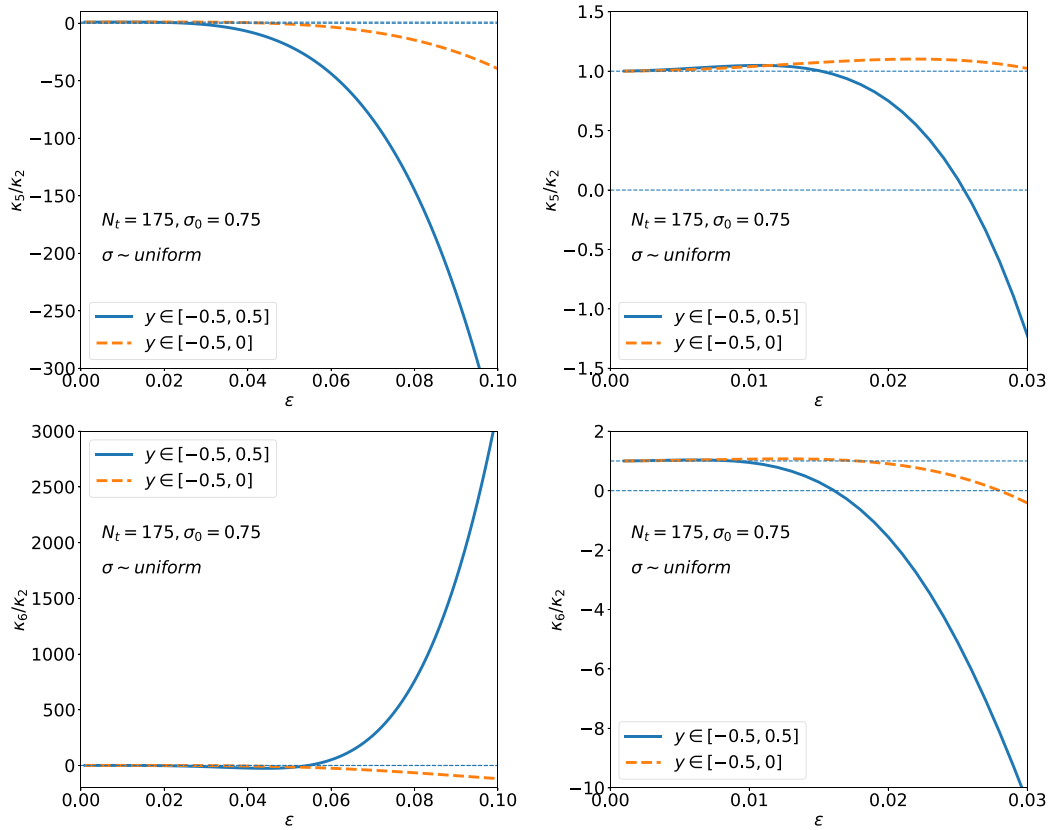


FIG. 12. κ_5/κ_2 and κ_6/κ_2 for σ following the uniform distribution. The left-hand side plots show wider ε range $[0, 0.1]$ whereas the right-hand side plots show details at small $\varepsilon \in [0, 0.03]$.

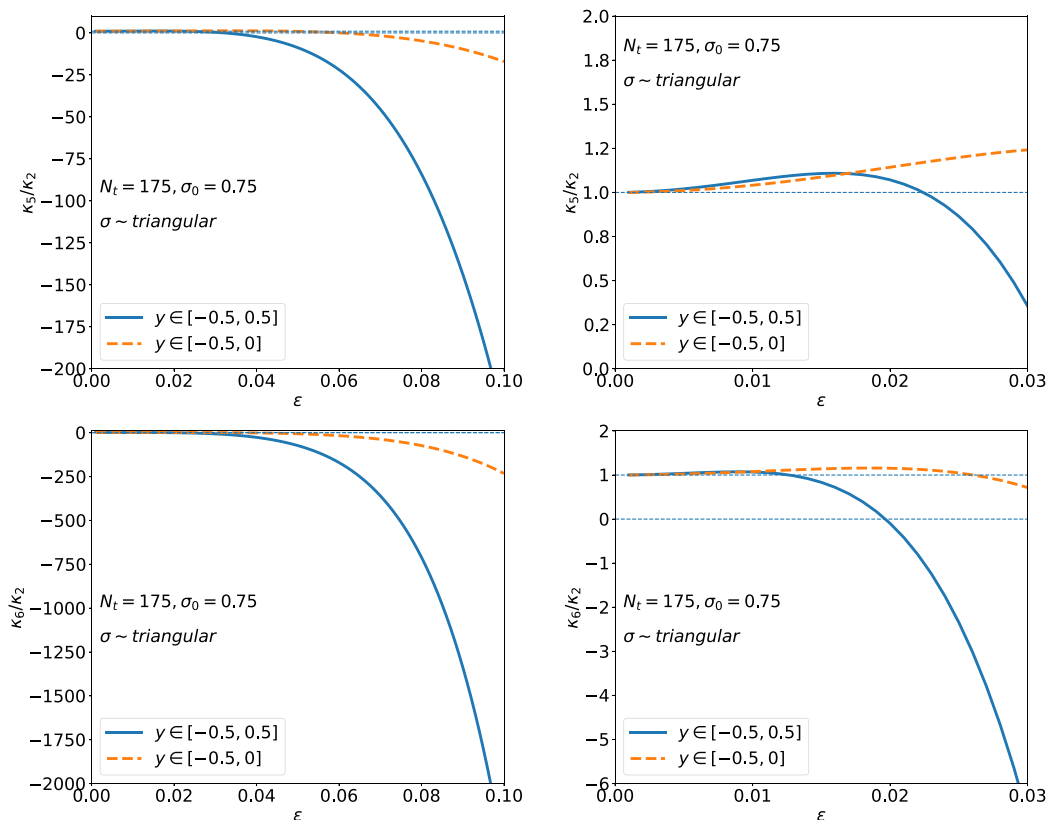
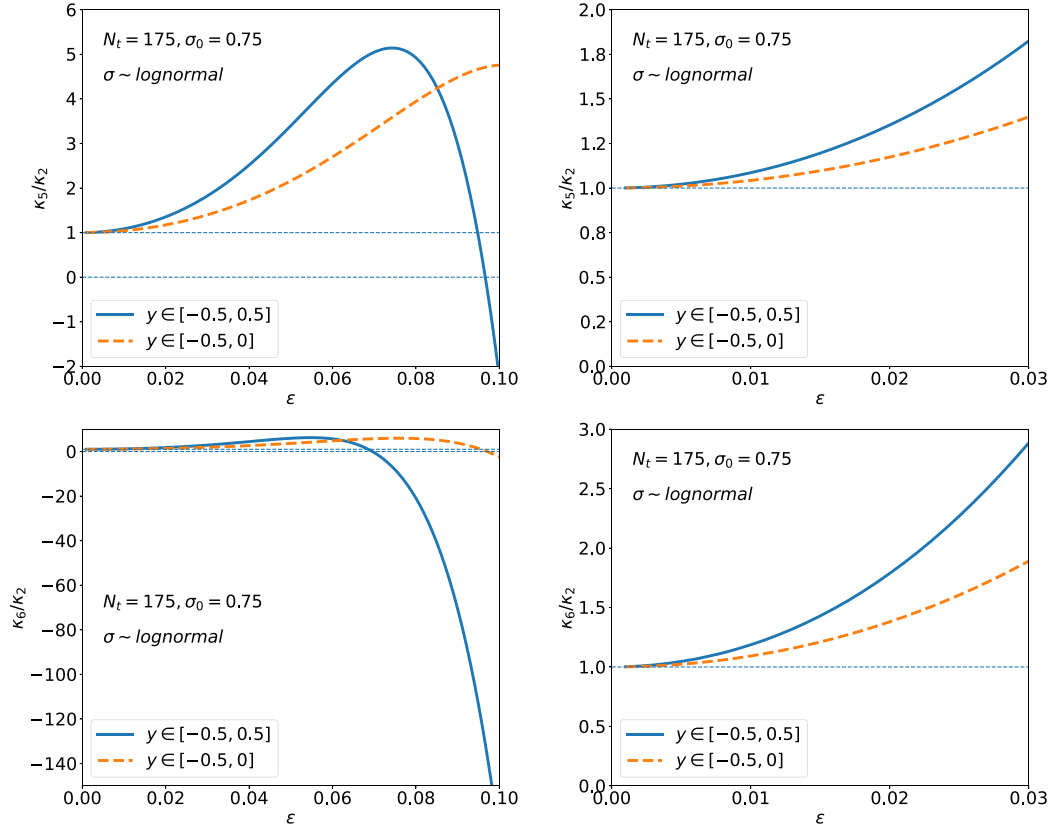


FIG. 13. Same as Fig. 12 but for σ following the triangular distribution.

FIG. 14. Same as Fig. 12 but for σ following the lognormal distribution.

- [1] J.-Y. Ollitrault, *Phys. Rev. D: Part. Fields* **46**, 229 (1992).
- [2] K. H. Ackermann *et al.* (STAR Collaboration), *Phys. Rev. Lett.* **86**, 402 (2001).
- [3] A. Bialas, A. Bzdak, and K. Zalewski, *Phys. Lett. B* **710**, 332 (2012).
- [4] A. Bzdak and D. Teaney, *Phys. Rev. C* **87**, 024906 (2013).
- [5] M. A. Stephanov, *Prog. Theor. Phys. Suppl.* **153**, 139 (2004).
- [6] P. Braun-Munzinger and J. Wambach, *Rev. Mod. Phys.* **81**, 1031 (2009).
- [7] P. Braun-Munzinger, V. Koch, T. Schäfer, and J. Stachel, *Phys. Rep.* **621**, 76 (2016).
- [8] A. Bzdak, S. Esumi, V. Koch, J. Liao, M. Stephanov, and N. Xu, *Phys. Rep.* **853**, 1 (2020).
- [9] X.-F. Luo, B. Mohanty, H. G. Ritter, and N. Xu, *Phys. At. Nucl.* **75**, 676 (2012).
- [10] S. Jeon and V. Koch, *Phys. Rev. Lett.* **85**, 2076 (2000).
- [11] M. Asakawa, U. W. Heinz, and B. Muller, *Phys. Rev. Lett.* **85**, 2072 (2000).
- [12] M. Gazdzicki, M. I. Gorenstein, and S. Mrowczynski, *Phys. Lett. B* **585**, 115 (2004).
- [13] M. I. Gorenstein, M. Gazdzicki, and O. S. Zozulya, *Phys. Lett. B* **585**, 237 (2004).
- [14] V. Koch, A. Majumder, and J. Randrup, *Phys. Rev. Lett.* **95**, 182301 (2005).
- [15] M. A. Stephanov, *Phys. Rev. Lett.* **102**, 032301 (2009).
- [16] M. Cheng *et al.*, *Phys. Rev. D* **79**, 074505 (2009).
- [17] W.-j. Fu, Y.-x. Liu, and Y.-L. Wu, *Phys. Rev. D* **81**, 014028 (2010).
- [18] V. Skokov, B. Friman, and K. Redlich, *Phys. Rev. C* **83**, 054904 (2011).
- [19] M. A. Stephanov, *Phys. Rev. Lett.* **107**, 052301 (2011).
- [20] C. Herold, M. Nahrgang, Y. Yan, and C. Kobdaj, *Phys. Rev. C* **93**, 021902(R) (2016).
- [21] X. Luo and N. Xu, *Nucl. Sci. Tech.* **28**, 112 (2017).
- [22] M. Szymański, M. Bluhm, K. Redlich, and C. Sasaki, *J. Phys. G* **47**, 045102 (2020).
- [23] C. Ratti, *PoS (LATTICE2018)*, 004 (2019).
- [24] N. K. Behera (ALICE Collaboration), *Nucl. Phys. A* **982**, 851 (2019).
- [25] J. Adamczewski-Musch *et al.* (HADES Collaboration), *Phys. Rev. C* **102**, 024914 (2020).
- [26] M. Abdallah *et al.* (STAR Collaboration), *Phys. Rev. C* **104**, 024902 (2021).
- [27] A. Bzdak and P. Bozek, *Phys. Rev. C* **93**, 024903 (2016).
- [28] J. Jia, S. Radhakrishnan, and M. Zhou, *Phys. Rev. C* **93**, 044905 (2016).
- [29] M. Rohrmoser and W. Broniowski, *Phys. Rev. C* **101**, 014907 (2020).
- [30] M. Aaboud *et al.* (ATLAS Collaboration), *Phys. Rev. C* **95**, 064914 (2017).

- [31] S. Acharya *et al.* (ALICE Collaboration), *Phys. Lett. B* **781**, 20 (2018).
- [32] R. Quishpe, Longitudinal fluctuations in relativistic heavy ion collisions, Ph.D. thesis, University of Houston, 2022.
- [33] B. Kimelman (STAR Collaboration), *Acta Phys. Pol. B Proc. Suppl.* **16**, 49 (2023).
- [34] The SciPy community, Scipy, version 1.10.1, <https://docs.scipy.org/doc/scipy/reference/generated/scipy.integrate.quad.html>, accessed: 27.01.2023.
- [35] B. Friman and K. Redlich, [arXiv:2205.07332](https://arxiv.org/abs/2205.07332).
- [36] M. S. Abdallah *et al.* (STAR Collaboration), *Phys. Rev. Lett.* **128**, 202303 (2022).
- [37] V. Vovchenko, V. Koch, and C. Shen, *Phys. Rev. C* **105**, 014904 (2022).
- [38] M. Abdallah *et al.* (STAR Collaboration), *Phys. Rev. C* **107**, 024908 (2023).
- [39] STAR Collaboration, Higher-order cumulants and correlation functions of proton multiplicity distributions in $\sqrt{s_{NN}} = 3$ GeV Au+Au collisions at the STAR experiment, HEPData (collection) (2023), <https://doi.org/10.17182/hepdata.134023>.
- [40] S. Acharya *et al.* (ALICE Collaboration), *Phys. Lett. B* **807**, 135564 (2020).
- [41] P. Braun-Munzinger, A. Rustamov, and J. Stachel, *Nucl. Phys. A* **960**, 114 (2017).
- [42] V. Skokov, B. Friman, and K. Redlich, *Phys. Rev. C* **88**, 034911 (2013).
- [43] A. Bzdak, V. Koch, and V. Skokov, *Phys. Rev. C* **87**, 014901 (2013).
- [44] P. Braun-Munzinger, B. Friman, K. Redlich, A. Rustamov, and J. Stachel, *Nucl. Phys. A* **1008**, 122141 (2021).
- [45] V. Vovchenko, O. Savchuk, R. V. Poberezhnyuk, M. I. Gorenstein, and V. Koch, *Phys. Lett. B* **811**, 135868 (2020).
- [46] M. Barej and A. Bzdak, *Phys. Rev. C* **102**, 064908 (2020).
- [47] M. Barej and A. Bzdak, *Phys. Rev. C* **106**, 024904 (2022).